Observation of diamagnetic effect in $BaSnO_3$ via low-temperature magneto-photoluminescence spectroscopy

2014 EPL 106 67005

(http://iopscience.iop.org/0295-5075/106/6/67005)

A Letters Journal Exploring the Frontiers of Physics

June 2014

EPL, **106** (2014) 67005 www.epljournal.org
doi: 10.1209/0295-5075/106/67005

Observation of diamagnetic effect in $BaSnO_3$ via low-temperature magneto-photoluminescence spectroscopy

Peng Zhang[1,2], Fuhai Su[1,3(a)], Jianming Dai[1(b)], Kejun Zhang[1], Chao Zhang[1], Wei Zhou[1], Qinzhuang Liu[1] and Li Pi[3]

[1] *Department 1Key Laboratory of Materials Physics, Institute of Solid State Physics, Chinese Academy of Sciences Hefei 230031, Anhui, PRC*
[2] *Department of Materials Science and Engineering, University of Science and Technology of China Hefei 230026, Anhui, PRC*
[3] *High Magnetic Field Laboratory, Chinese Academy of Sciences - Hefei 230031, Anhui, PRC*

received 17 January 2014; accepted in final form 28 May 2014
published online 18 June 2014

PACS 75.20.-g – Diamagnetism, paramagnetism, and superparamagnetism
PACS 71.20.Dg – Alkali and alkaline earth metals
PACS 78.55.-m – Photoluminescence, properties and materials

Abstract – Photoluminescence measurements for pure $BaSnO_3$ are carried out at low temperatures and high magnetic fields, down to 4 K and up to 8 T, respectively. Multiple phonon replicas are observed in the near-infrared region, which allows for a quantitative estimation of the Huang-Rhys factor, $S = 3.0$. Due to the extremely narrow linewidth, a magnetic-field–induced nonlinear blueshift of the zero phonon line (ZPL) and a small increase of the phonon energy are clearly distinguishable. The magnetic-field dependence of the ZPL energies can be interpreted in terms of diamagnetic effects of the *s*-like local electronic state. The electron effective mass value of $0.14m_0$ is extracted from the best fitting.

Barium stannate ($BaSnO_3$) is a transparent semiconductor with an optical gap larger than 3.1 eV [1,2] that, with appropriate doping modulation, holds tremendous promise in many applications, including gas sensing [3], photo-catalysis [4,5], spintronics [6], and thermally stable capacitors [7]. In order to develop sophisticated semiconductor devices based on $BaSnO_3$, it is crucial to understand the fundamental physics of the material such as electron-phonon interactions, its electronic structure, and electric-magnetic interactions. In recent years, extensive pioneering works have been dedicated to doped and undoped $BaSnO_3$, exploring material fabrication [2,8], band structure [9,10], optical properties [2,10], and electronic transport [1]. We have investigated changes to the optical band gap and electrical conductivity induced in $BaSnO_3$ films by strontium and lanthanum ion doping, respectively [2,11]. However, many basic properties and parameters, *e.g.*, the mageto-optics effect, the electron-phonon coupling strength, carrier effective masses, etc., have been relatively unexplored experimentally to date. Recently, a few studies [12] have investigated the photoluminescence (PL) spectra of pure or doped $BaSnO_3$ and reported strong photon emission at around 900 nm, which shed light on the potential for $BaSnO_3$-based conductors to be used as opto-electronic devices in the near-infrared region. To pave the way for future applications, a deeper understanding of the near-infrared (NIR) luminescence is required. Measurements of the PL spectrum under strong external magnetic fields and at low temperatures provide valuable information about the interactions between electron excitations and phonons or magnetons. The externally applied magnetic field breaks the degeneracy of spin states or induces a diamagnetic energy in an optically excited semiconductor system, which can be revealed by analyzing the lineshape, polarization, and intensity of the magnetic-field–dependent PL spectrum. The energy changes due to the diamagnetic or spin-split effect under moderate (1–10 tesla), and even higher, magnetic fields normally fall into the range of a few meV. However, the PL linewidth in most bulk semiconductors can reach hundreds of meV at room temperature, mainly due to electron-phonon interactions and thermal smearing. This broad spectrum limits the precise detection of

(a) E-mail: fhsu@issp.ac.cn
(b) E-mail: jmdai@issp.ac.cn

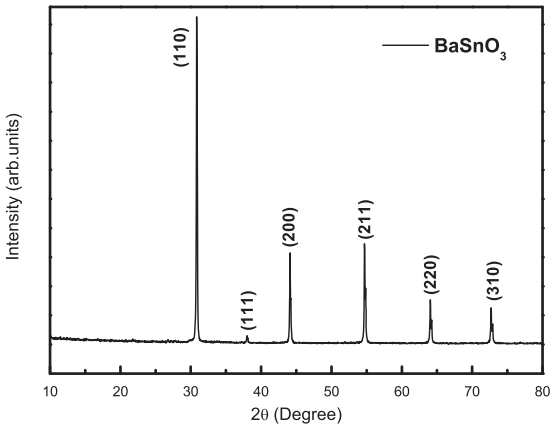

Fig. 1: XRD pattern for $BaSnO_3$ at room temperature.

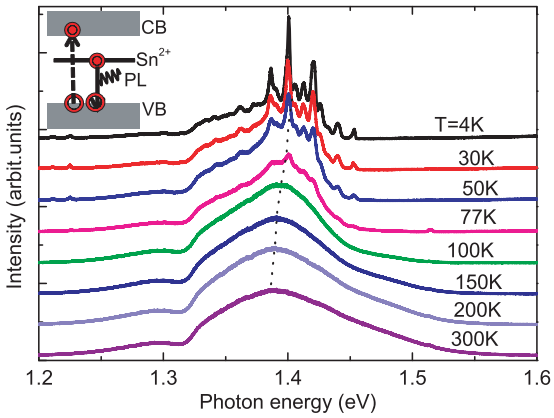

Fig. 2: (Colour on-line) Photoluminescence spectra at different temperatures. The dashed line is a guide to the eye indicating the peak positions. The inset illustrates the irradiative recombination process from the deep level to the valence band.

magnetic-field–induced energy shifts and the splitting of emission peaks. Fortunately, when the lattice temperature is sufficiently low, the phonons involved in the electronic transition can be suppressed and lattice vibration quantization can enable the formation of sequential emission lines with extremely narrow linewidths in some materials. As demonstrated in earlier work on the green emission in ZnO [13], the fine structure of emission bands can provide access to tiny magnetic energies via identification of changes to the PL spectrum under moderate magnetic fields. In this work, we focus on the PL structure near 900 nm in pure $BaSnO_3$ at temperatures down to 4 K and external magnetic fields up to 8 tesla. We present the first investigation of the multiple phonon emission lines in $BaSnO_3$. We detect the energy blueshifts of less than 1 meV thanks to the sharp zero-order emission line. The blueshifts have a quadratic magnetic-field dependence, which is found to arise from the diamagnetic shift of a deep electronic state.

The polycrystalline sample of $BaSnO_3$ was synthesized with a conventional solid-state reaction method. The starting high-purity $BaCO_3$ and SnO_2 powers were weighed in the stoichiometric ratio and then mixed thoroughly. The mixtures were placed into Al_2O_3 crucibles and then calcined in air at 1200 °C for 48 h. The resultant powders were ground and pressed into small pellets. The obtained pellets were then sintered at 1350 °C for 24 h, followed by another 24 h annealing at 1450 °C with an intermediate grinding. In the end, the pellets were ground into homogeneous powder samples. X-ray diffraction (XRD) studies were carried out at around 300 K using an X-ray diffractometer with Cu K_α radiation (PHILIPS, $\lambda = 0.15406$ nm) to determine the crystal structure. The PL was excited by a He-Cd laser at a wavelength of 325 nm. The emitted light was analyzed and detected by a spectrometer (Princeton action SP2500, equipped with a CCD detector) with a resolution of 0.08 nm and a scan range of 300–1400 nm. A superconducting magnet (Oxford Spectromag SM4000) was used to exert the magnetic field and cool down samples. The magnetic field and temperature can be varied in a range of 0–8 T and 4–300 K, respectively. During the measurement the sample was mounted on a cold finger and the optical path for light collection was parallel to the magnetic-field direction.

Figure 1 shows the XRD result of the pure $BaSnO_3$ powder sample. All diffraction peaks can be indexed as cubic perovskite $BaSnO_3$ (JCPDS card No. 15-0780) with the $Pm\bar{3}m$ space group, and there are no detectable secondary phases. In fig. 2, the PL spectra under different temperatures with zero magnetic field are presented. Mizoguchi *et al.* [12] first observed a broad emission band centered at around 1.38 eV (900 nm) in the temperature range between 77 K and 300 K. The extraordinary NIR luminescence band was assigned to irradiative recombination from an occupied donor level related to the Sn^{2+} ions to a photogenerated valence band hole [12]. As the temperature increases, the mass centers of the spectra shift slightly toward the low-energy region. The observed redshift may result from the valence band changes induced by the lattice thermal expansion. When the sample is cooled to temperatures lower than 77 K, multiple sharp emission lines with bandwidths of a few meV are superposed on the spectrum, as can be clearly seen in fig. 2. These lines arise from electronic transition accompanied by phonon emission.

To further clarify the origin of the fine features, the spectrum at 4 K temperature and zero magnetic field is plotted again in fig. 3, where the logarithmic vertical axis allows the fine emission structure to be resolved more clearly. As shown in fig. 3, the discrete emission structure is comprised of a series of separated emission lines and can even be tracked to the low-energy tail of the spectrum, as marked by arrows. The groups of lines labeled as 5-, 4-, 3-, 2-, 1-ph and ZPL, which have equal energy intervals of 13 meV between adjacent peaks, can be clearly distinguished in the fine structure of the luminescence. The 4-line has the maximum intensity. The energy separation is close to the low-frequency phonon mode with 115 cm^{-1}

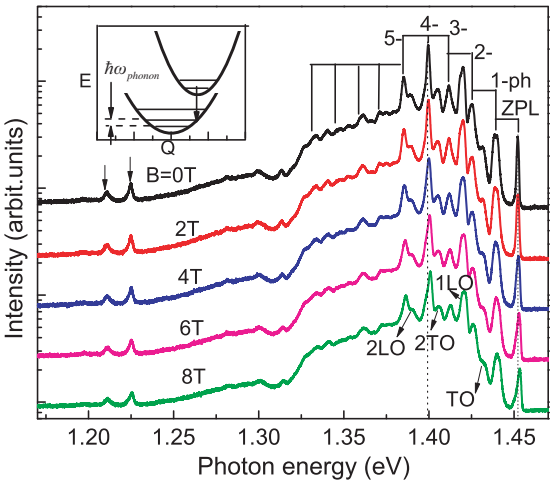

Fig. 3: (Colour on-line) Magnetic-field–dependent photoluminescence spectra measured at a temperature of 4 K. The vertical dotted lines are plotted as a guide for the eye. The inset represents the coordinate configuration diagram of the ground and the excited states that differ in their configuration due to the electron-phonon coupling. The electronic transitions along with the multiple phonon emission take place in terms of $E_n = E_{ZPL} - n\hbar\omega_{phonon}$.

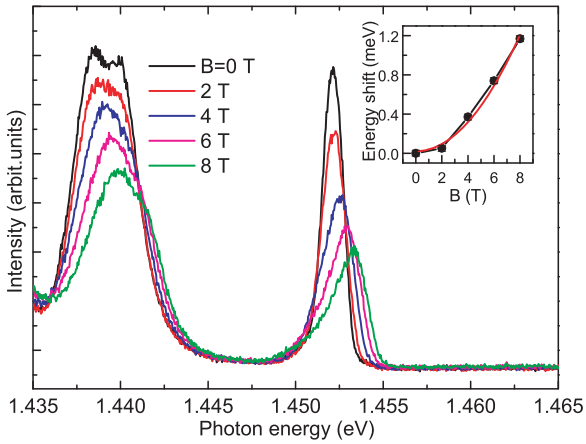

Fig. 4: (Colour on-line) The selected PL spectra zone from fig. 3 *vs.* magnetic field. In order to demonstrate the PL energy shift more clearly, the spectra only cover the zero-order lines and the first-order phonon replicas. In the inset, the ZPL energies are shown as a function of the magnetic field, where the solid line comes from the fitting according to eq. (3).

energy measured using the Raman scattering [14]. This phonon mode may be connected to the vibration of Ba ions, as indicated by the recent first-principles calculation on the infrared spectrum of $BaSnO_3$ [10]. The consistency between the spacing of the emission peaks and the phonon mode suggests that the fine-structure features correspond to multiple phonon emission lines [15]. The phonon emission process is linked to recombination through the Franck-Condon configuration, as illustrated in the inset in fig. 3. The *s*-like electronic state of Sn^{2+} ions, which is possibly due to the Sn-O-Sn bending or dislocation of Sn ions [12], serves as a local donor state in the band gap. Its lattice coordinate configuration is displaced relative to the valance band, which is dominated by the electronic *p* states of oxygen ions. The coordinate shift enables the electronic transitions from the Sn^{2+} donor states at the lowest lattice vibration level to the photoexcited-hole states at sequentially quantized phonon modes. As a result, the zero phonon line (ZPL) at energy E_{ZPL} is accompanied by a phonon replica below E_{ZPL} at integer multiples of the phonon energy $\hbar\omega_{phonon}$ at low temperature, *i.e.*,

$$E_n = E_{ZPL} - n\hbar\omega_{phonon}. \quad (1)$$

Here the peak with a maximum energy of 1.4 eV can be assigned as ZPL and the phonon mode involved has an energy of 13 meV. It is well known that the linear electron-phonon approximation gives a quantitative description to the integrated intensity I_n of the n-th phonon replica as [15]

$$I_n \propto \exp(-S)\frac{S^n}{n!}. \quad (2)$$

The Huang-Rhys factor, S, is directly proportional to the coupling strength between the excited electronic state and the phonon. According to the above expression, the Huang-Rhys factor can be obtained from the intensity of these phonon replicas. However, it is hard to extract the integrated intensity of a single peak for high-order phonon replicas since the phonon emission lines from other phonon mode blur their lineshapes. Here we determine that $S = 3.0 \pm 0.3$ based on the integrated intensity ratio of the first-order phonon replica to the ZPL. In the low-lying phonon sideband, we can also resolve another two groups of phonon replicas with 20 meV and 33 meV spacing, respectively. The obtained phonon energies are close to the TO and LO phonon modes measured by Raman spectra [14]. As expected, these different phonon replicas merge into a continuous broad envelope due to thermal smearing with increasing temperature, as demonstrated in fig. 2. However, the temperature-induced spectral broadening exhibits an asymmetric evolution: there is a pronounced stretch toward the high-energy side, but the low-energy wing of the profile does not obviously change, which may be associated with the influence of the temperature on the phonon thermal distribution.

In fig. 3, the PL spectra under different magnetic fields are plotted. All the sharp phonon replicas move toward the blue side with increasing external magnetic field. A magnified view of the portions of the spectra covering the ZPLs and the 1st-order phonon emission lines are presented as a function of the magnetic field in fig. 4. As the magnetic field increases, the intensities of the ZPL and phonon sidebands tend to decay significantly. Meanwhile, the ZPL lineshape is broadened asymmetrically. The PL darkening effect may originate from a magnetic-field–induced localization of the wave function. The wave functions of both *s*-like local donor states and photoexcited hole states in the valance band tend to be compressed

spatially under a high magnetic field. Consequently, the wave function overlap and transition probability between the donor state and the valence band is expected to decrease with increasing magnetic field. In addition to the lineshape changes, a tiny blueshift of less than 1 meV can be clearly identified due to the extremely narrow bandwidth of the ZPL and phonon replicas. The ZPL energies are plotted as a function of the magnetic field in the inset of fig. 4, and exhibit a typical nonlinear magnetic-field dependence. As for the mechanisms that are possibly responsible for the NIR ZPL blueshift in $BaSnO_3$, we primarily excluded the Zeeman effect based on the following two reasons. First, we did not observe the spectrum splitting that is characteristic of the Zeeman quantization. Second, the observed parabolic magnetic-field dependence of the emission energies deviates from the linear relation described by the Zeeman energy shift, whose slope characterizes the g factor in a material. We propose that the diamagnetic effect accounts for the nonlinear magnetic-field dependence of the ZPL energy. Since the Sn^{2+} ion donor state is occupied by two paired $5s$ electrons, the energy term contributed by the magnetic momentum should be zero under a magnetic field. In this case, the diamagnetic energy increase, $\Delta\varepsilon$, of the s-like local state with magnetic field (B) has the following form in the weak-field approximation [16]:

$$\Delta\varepsilon = \frac{4\pi^2\varepsilon_r^2\varepsilon_0^2\hbar^4}{e^2m^{*3}}B^2. \quad (3)$$

Here ε_r and m^* correspond to the relative dielectric constant and electron effective mass, respectively. We apply the above quadratic expression to fit the experimental ZPL energies that vary with the magnetic field and then extract the effective mass, $m^* = (0.14 \pm 0.01)m_0$, from the best agreement by introducing the dielectric constant reported in the literature, $\varepsilon_r = 20$ [17]. Here m_0 denotes the free electron mass. It should be mentioned that the magnetic-field–induced Landau-level change in the valence band should be negligible because of the following two considerations: i) Our sample is a polycrystalline powder, and the inhomogeneity in the crystalline grains would destroy the cyclotron orbits. ii) The cyclotron period of hole in valence band would be a few picoseconds under 8 T magnetic field because its effective mass is higher than that of the electron. This time scale is far longer than the scattering time (a few hundred femtoseconds in bulk), which means that holes fail to complete a cyclotron orbit and thus form a Landau level before scattering occurs.

Next we derived the phonon energies involved in the NIR transition from the interval between the ZPL and the first-order replica as a function of the magnetic field, which is displayed in fig. 5. The magnetic-field–dependent Huang-Rhys factors are also extracted by analyzing the integrated intensity of the emission lines. It is interesting that the obtained phonon energy is increased by about 0.3 meV when the magnetic field approaches 8 T. The influence of the magnetic field on the lattice vibrations

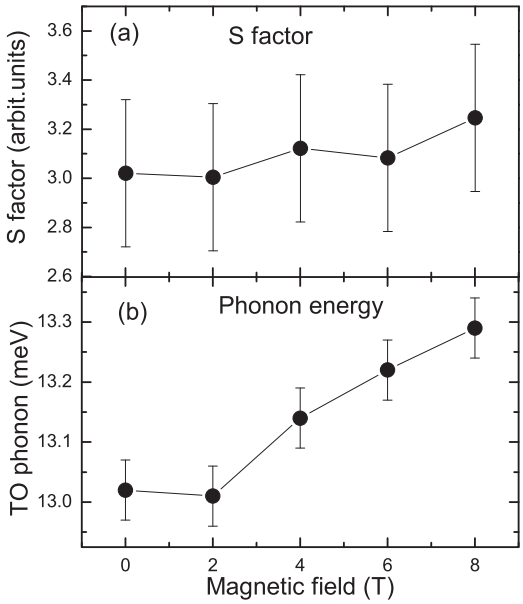

Fig. 5: The magnetic-field dependence of the extracted Huang-Rhys factors (a) and phonon energies (b).

in $BaSnO_3$ needs elaborate further investigations with magento-optical Raman spectroscopy. Here we tentatively suggest that the phonon energy change may be associated with the change of the electron momentum induced by the magnetic field. In the presence of a magnetic field, the electron momentum is modified by the vector potential, eA, and, thereby, the phonon participating in the electronic transition requires an appropriately modified wave vector in order to maintain momentum conservation. Consequently, the wave vector change of the corresponding phonon mode leads to the phonon energy modification due to phonon dispersion. In addition, it is worth noting that the estimated S factors do not show a clear magnetic-field dependence, which emphasizes that electron-phonon coupling is independent of the magnetic field in the applied field range.

In summary, we performed PL measurements for pure $BaSnO_3$ at low temperatures and under external magnetic fields up to 8 tesla. Phonon sidebands composed of multiple phonon emission features as well as a zero phonon line are observed in the NIR region at low temperature. From the intensity ratio between the 1st phonon replica and the ZPL, the Huang-Rhys factor, $S = 3.0$, is extracted. The sharp PL features also allow for a precise detection of the magnetic energy of the excited electronic state. We observed a blueshift of the peak energies of the ZPL and its replicas as we increased the magnetic field. The parabolic magnetic-field dependence can be well described in terms of the diamagnetic effect of s-like Sn^{2+} excited states, and the effective mass of $0.14m_0$ can be determined from a simple simulation. In addition, the phonon mode involved in the electronic transition presents a light increase in energy with the magnetic field. However, the Huang-Rhys factors show weak magnetic-field dependence.

* * *

The authors would like to thank Dr T. L. Cocker for helpful discussions and for a critical reading of the manuscript. This work was supported by the National Natural Science Foundation of China (Grant Nos. 11004199, 11004071, 11374304).

REFERENCES

[1] Luo X., Oh Y. S., Sirenko A., Gao P., Tyson T. A., Char K. and Cheong S.-W., *Appl. Phys. Lett.*, **100** (2012) 172112.
[2] Liu Q. Z., Li B., Liu J. J., Li H., Liu Z. L., Dai K., Zhu G. P., Zhang P., Chen F. and Dai J. M., *EPL*, **98** (2012) 47010.
[3] Ostrick B., Fleischer M., Lampe U. and Meixner H., *Sens. Actuators B*, **44** (1997) 601.
[4] Borse P. H., Joshi U. A., Ji S. M., Jang J. S., Lee J. S., Jeong E. D. and Kim H. G., *Appl. Phys. Lett.*, **90** (2007) 034103.
[5] Yuan Y., Lv J., Jiang X., Li Z., Yu T., Zou Z. and Ye J., *Appl. Phys. Lett.*, **91** (2007) 094107.
[6] Balamurugan K., Harish Kumar N., Ramachandran B., Ramachandra Rao M. S., Arout Chelvane J. and Santhosh P. N., *Solid State Commun.*, **149** (2009) 884.
[7] Singh P., Kumar D. and Parkash O., *J. Appl. Phys.*, **97** (2005) 074103.
[8] Azad A.-M. and Hon N. C., *J. Alloys Compd.*, **270** (1998) 95.
[9] Deepa A. S., Vidya S., Manu P. C., Solomon Sam, John Annamma and Thomas J. K., *J. Alloys Compd.*, **509** (2011) 1830.
[10] Moreira E., Henriques J. M., Azevedo D. L., Caetano E. W. S., Freire V. N., Fulco U. L. and Albuquerque E. L., *J. Appl. Phys.*, **112** (2012) 043703.
[11] Liu Q. Z., Liu J. J., Li B., Zhu G. P., Li H., liu Z. L., Dai K., Zhang P. and Dai J. M., *Appl. Phys. Lett.*, **101** (2012) 241901.
[12] Mizoguchi H., Woodward P. M., Park C.-H. and Keszler D. A., *J. Am. Chem. Soc.*, **126** (2004) 9796.
[13] Dingle R., *Phys. Rev. Lett.*, **23** (1969) 579.
[14] Stanislavchuk T. N., Sirenko A. A., Litvinchuk A. P., Luo X. and Cheong S.-W., *J. Appl. Phys.*, **112** (2012) 044108.
[15] Grundmann M., *The Physics of Semiconductors: An Introduction Including Devices and Nanophysics* (Springer, Heidelberg) 2006, p. 264.
[16] Miura N., *Physics of Semiconductors in High Magnetic Fields* (Oxford University Press, United Kingdom) 2008, p. 54.
[17] Singh P., Brandenburg B. J., Sebastian C. P., Singh P., Singh S., Kumar D. and Parkash O., *Jpn. J. Appl. Phys.*, **47** (2008) 3540.